PCCP

RSCPublishing

PAPER

Cite this: DOI: 10.1039/x0xx00000x

Received 00th January 2012,
Accepted 00th January 2012

DOI: 10.1039/x0xx00000x

www.rsc.org/

# Stochastic methods for aerosol chemistry: a compact molecular description of functionalization and fragmentation in the heterogeneous oxidation of squalane aerosol by OH radicals

A. A. Wiegel,[a] K. R. Wilson,[a]* W. D. Hinsberg,[b] and F. A. Houle [a]*

The heterogeneous oxidation of organic aerosol by hydroxyl radicals (OH) can proceed through two general pathways: functionalization, in which oxygen functional groups are added to the carbon skeleton, and fragmentation, in which carbon-carbon bonds are broken, producing higher volatility, lower molecular weight products. An ongoing challenge is to develop a quantitative molecular description of these pathways that connects the oxidative evolution of the average aerosol properties (e.g. size and hygroscopicity) to the transformation of free radical intermediates. In order to investigate the underlying molecular mechanism of aerosol oxidation, a relatively compact kinetics model is developed for the heterogeneous oxidation of squalane particles by OH using free radical intermediates that convert reactive hydrogen sites into oxygen functional groups. Stochastic simulation techniques are used to compare calculated system properties over ten oxidation lifetimes with the same properties measured in experiment. The time-dependent average squalane aerosol mass, volume, density, carbon number distribution of scission products, and the average elemental composition are predicted using known rate coefficients. For functionalization, the calculations reveal that the distribution of alcohol and carbonyl groups is controlled primarily by the initial OH abstraction rate and to lesser extent by the branching ratio between secondary peroxy radical product channels. For fragmentation, the calculations reveal that the formation of activated alkoxy radicals with neighboring functional groups controls the molecular decomposition, particularly at high O/C ratios. This kinetic scheme provides a framework for understanding the oxidation chemistry of a model organic aerosol and informs parameterizations of more complex systems.

## 1. Introduction

The atmosphere of Earth contains a staggering number of organic compounds with an estimated hundreds of thousands of individual species.[1] Many of these organic compounds participate in the formation and evolution of particulate matter, as components of aerosol, as secondary organic aerosol (SOA) precursors, or as both. Since organic particulate matter impacts cloud properties, air quality, human health, and climate, a detailed description of its chemical evolution in the atmosphere is crucial for making quantitative predictions of its concentrations and of the influence of human activity. However, a detailed description of the chemical transformations of such a large number of chemical species is enormously challenging, since the number of combinations of reactants and the number of oxidation reaction pathways becomes intractable even when starting with a single organic compound and a single oxidant under controlled laboratory conditions. Given the complexity of describing each species and their accompanying reaction pathways explicitly, several parameterizations have been developed for understanding the formation and chemical evolution of organic aerosol.[2–9] These approaches are based on bulk measurable average aerosol properties such as elemental ratios,[3] carbon oxidation state,[5] polarity,[6] volatility,[2,7] electron impact ionization marker ions,[8] or multigenerational statistical

oxidation.[9] Such parameterizations are more tractable ways of describing how oxidation transforms the physiochemical properties (i.e. size, hygroscopicity, volatility, etc.) of the organic aerosol. However, they often lack a concrete and quantitative connection between the underlying oxidation mechanisms — often involving multiple generations of free radical intermediates — and the transformation of average organic aerosol properties.

Previous experimental kinetics work has shown two general reaction pathways for organic aerosol upon oxidation by OH radicals: functionalization, which adds additional oxygen functional groups to the carbon skeleton, and fragmentation, which leads to C-C bond scission and lower molecular weight oxidized products.[10] Furthermore, the "branching ratio" between these two pathways was found to be dependent on molecular structure, with more branched and more oxidized hydrocarbons undergoing more fragmentation than functionalization.[11,12] For both of these oxidation pathways, the central intermediate is an organic peroxy radical ($RO_2$), formed from the addition of molecular oxygen to the alkyl radical formed via hydrogen abstraction by OH as shown in Figure 1.. Peroxy radicals undergo several possible self-reactions[13–15] to form alcohols, ketones, and alkoxy radicals. While all of these peroxy reactions will result in functionalized products, $\beta$-scission of an alkoxy radical (R6) is the only known pathway that leads to fragmentation products.[16] The reaction scheme shown in Figure 1. is largely based on gas phase studies of the reactions of organic peroxy radicals, and to what extent these gas phase mechanisms for hydrocarbon oxidation can be reliably applied to heterogeneous or bulk phase oxidation remains unclear. In particular, oxidation within the bulk liquid phase is heavily influenced by the presence of the solvent cage, which may depress chemistry common to the gas phase while promoting reactions that would not otherwise occur in the gas phase.

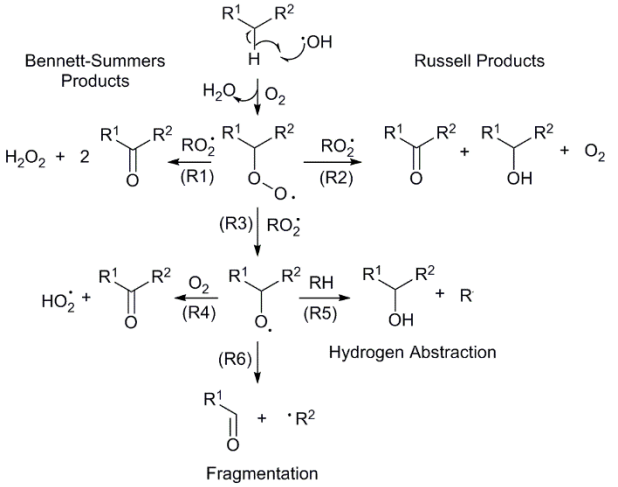


Figure 1. Generalized reaction scheme for the oxidation of hydrocarbons by OH in the absence of $NO_x$. An expanded representation of (R1), (R2), and (R3) is shown in Figure 2..

Previous studies of peroxy radical self-reactions in the condensed phase showed that the reaction proceeds through a tetroxide ($RO_4R$) intermediate. Based on measurements hydrogen-deuterium isotope effects, Russell[17] concluded that the self-reaction of peroxy radicals generated from arylalkyl hydrocarbons proceeds through a cyclic transition state, leading to equal parts alcohol and ketone as shown in (R2). Indeed, gas phase product studies of $RO_2$ self-reactions show that alcohols and ketones are formed in equal yields.[13–15] Later condensed phase studies of the oxidation of alkanes showed that the reaction actually favored ketones over alcohols at room temperature as in (R1), with more ketones at lower temperatures and more alcohols at higher temperatures.[18] These results suggested that the one to one ratio of ketones and alcohols observed by Russell[17] was a special case and that the ratio could vary depending on molecular structure. For aerosols, heterogeneous oxidation of various single component particles such as squalane and bis(2-ethylhexyl)sebacate suggests that ketones are indeed favored in the self-reaction of $RO_2$ radicals,[10,19] although some have thought that the reaction of alkoxy radicals with $O_2$ to form ketones (R4) could also be surface-enhanced.[20]

Denisov[21,22] proposed an alternative mechanism for the self-reaction of peroxy radicals shown in Figure 2. that is consistent with the observed products and other experimental and theoretical data for the peroxy termination reactions. In contrast to the cyclic intermediates proposed by Russell[17] and the anti-cyclic intermediate proposed by Bennett and Summers,[18] Denisov suggested that the tetroxide intermediate first undergoes homolytic cleavage to form an alkoxy radical and a trioxide radical as the rate-limiting step. Because of the presence of the solvent cage in the condensed phase, primary and secondary peroxy radicals can undergo further reactions to form two ketones and hydrogen peroxide (R1); an alcohol, a ketone, and oxygen (R2); or two alkoxy radicals and oxygen (R3). Importantly, because of the presence of the radical cage, the formation of "free" alkoxy radicals, which are thought to be responsible for fragmentation in aerosol, has a much lower branching ratio (~5-10%)[23] in the condensed phase compared with the branching ratio for the gas phase formation of alkoxy radicals (~60-90%).[13] This mechanism also implies that the "Russell mechanism" and the "Bennett-Summers mechanism" are not actually separate mechanisms, but rather the product branching ratio of the $RO_2$ + $RO_2$ reaction depends on molecular structure and temperature. While this mechanism is consistent with the observed products and other experimental data for oxidation experiments of hydrocarbons, whether it can also be applied to the heterogeneous reactions on aerosol by gas phase radicals remains unclear.

 

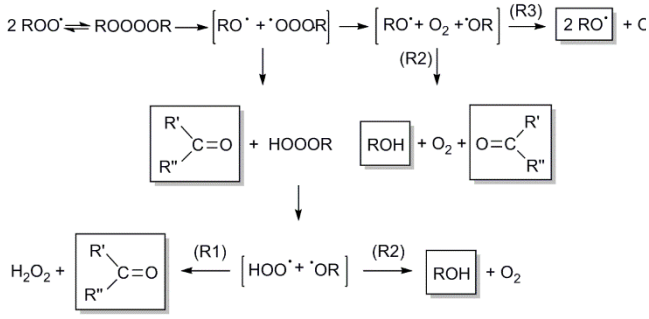


Figure 2. Reaction mechanism for the disproportionation of two peroxy radicals. Square brackets represent the radical cage, and boxes represent stable products. Note that when both R groups are tertiary, only the alkoxy radical formation reaction (R3) is possible because of the lack of *α*-hydrogens on R.

To analyze the different possible reaction pathways for the heterogeneous oxidation of organic aerosol and to test different possible mechanisms, a chemical kinetics model is developed and used to study the first ten oxidation lifetimes of the model heterogeneous reaction: OH + squalane. This system is chosen because of the rich array of experimental data available from previous studies.[10,11,24] Due to the large quantity of experimental data, the model predictions can be compared to the aerosol mass, elemental ratios, fragment product distributions, and other measurements to validate and explore the reaction mechanisms of free radicals in organic aerosol. Through this study, we develop a molecular level description of the mechanisms of aerosol oxidation that provides a more universal understanding of how organic aerosol ages in the atmosphere.

An overview of this study follows here. The methods used to develop the model are given in section 2. The stochastic simulation method is briefly described along with the overall approach to modeling the kinetics of this reaction (2.1). Then, the chemistry of the initial OH abstraction and formation of peroxy radicals (2.2), the bimolecular reactions of peroxy radicals (2.3), the decomposition of alkoxy radicals (2.4), and the evaporation of smaller carbon number products (2.5) are each described in more detail. In section 3, the results of the simulation are compared with experiment to examine which kinds of chemistry are important for understanding the functionalization (3.1) and fragmentation (3.2) mechanisms in organic aerosol. Finally, the significance of these model results for the aging of atmospheric aerosol and key features of the underlying mechanism are discussed in section 4.

## 2. Methods

### 2.1. Simulation Method

For this work, a chemical kinetics model is developed and solved using stochastic simulation methods instead of the more typical approach that employs deterministic coupled differential equations.{FormattingCitation}[25,26] Stochastic algorithms,[27,28] originally developed in the 1970s, are a subclass of kinetic Monte Carlo simulations that conduct a random walk through reaction event space instead of physical space to generate a time history of the studied system. The program used for the simulations is called *Kinetiscope* and is an enhanced version of the CKS and VSIM codes used in previous work.[29–31] This simulation package has been used to successfully describe key aspects of materials chemistry, from rare events controlled by coupled equilibria[32,33] to coupled reaction-diffusion processes on surfaces.[30] The simulations generate an absolute time base, enabling direct comparison of the concentrations and other system properties as a function of time to experimental data. Most importantly, because the algorithm involves simple arithmetic to advance the simulation instead of integration of coupled differential equations, molecules can be represented as whole or partial species. Thus, complex systems can be simulated in a very flexible manner, which we have exploited in this work. Because squalane aerosol is well-mixed (i.e. concentrations are uniform throughout the particle) on the timescale of the experiment, we represent the system as a single compartment with a volume given by the measured average diameter of the experimental particle size distribution. Since the volume decreases over the experiment due to increasing chemical densities and evaporation, we can also track its value volume continually throughout the simulation and update the concentrations of all chemical species accordingly. This moving boundary is straightforward to include using the stochastic method and is essential to obtaining good agreement with experiment. Using these techniques, we construct a mechanism that allows us to explore the oxidation chemistry to further refine and understand its characteristics in the liquid phase.

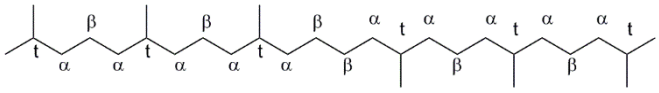


Figure 3. The molecular structure of squalane, showing tertiary, *α*-secondary, and *β*-secondary sites as defined for the model.

We consider the chemical transformations of the squalane aerosol from its initial unreacted state through the molecular processes of functionalization and fragmentation. We simplify the model by embedding an implicit adsorption step in the initial hydrogen abstraction by OH using the reactive uptake coefficient, *γ*, to calculate a pseudo-first order rate coefficient. This description of uptake is valid for single compartment simulations where mixing is assumed to be instantaneous, but is not applicable to full reaction-diffusion models.[34] The subsequent reaction steps are outlined in Figure 1., which includes peroxy formation, peroxy-peroxy reactions, and alkoxy formation. Once formed, alkoxy radicals can undergo hydrogen abstraction or fragmentation. The products from the fragmentation reaction can subsequently evaporate from the particle to form gas phase products. Wherever possible, literature rate constants are used directly or derived from measurements. Where rate constants and product branching ratios do not

exist, we describe how we have estimated them. Using these rate coefficients, an absolute time history for the oxidation process is calculated, enabling a direct comparison of the simulated and the measured aerosol mass, density, volume, average chemical composition, and carbon fragment distribution. The model-measurement agreement or disagreement is used to refine the overall description of the chemical mechanism by modifying the sequence of steps included.

Table 1. Model parameters and their initial values

| Parameter | Description | Initial Value |
|---|---|---|
| $d_p$ | Diameter of the particle | 160 nm |
| $\rho_0$ | Density of the particle | 0.81 g cm$^{-3}$ |
| $\gamma_{OH}$ | Reactive uptake of OH | 0.26 |
| [$O_2$(g)] | Gas phase concentration of $O_2$ | $1.23 \times 10^{18}$ cm$^{-3}$ |
| [OH(g)] | Gas phase concentration of OH | $10^{11}$ cm$^{-3}$ |
| [C30] | Concentration of squalane | $1.154 \times 10^{21}$ cm$^{-3}$ |
| [*tert*-H] | Concentration of tertiary hydrogen | $6.924 \times 10^{21}$ cm$^{-3}$ |
| [$\alpha$-H] | Concentration of $\alpha$-secondary hydrogen | $2.038 \times 10^{22}$ cm$^{-3}$ |
| [$\beta$-H] | Concentration of $\beta$-secondary hydrogen | $1.385 \times 10^{22}$ cm$^{-3}$ |
| [*prim*-H] | Concentration of primary hydrogen | $2.770 \times 10^{22}$ cm$^{-3}$ |

The reaction mechanism for oxidation of aerosol quickly becomes complex, even when starting from a single component such as squalane. For example, if the types of products from the first generation of oxidation of squalane were only limited to ketones, secondary alcohols, and tertiary alcohols without considering each individual isomer, by the fifth generation of oxidation the number of combinations of isomers from each generation for these three types of products is 56. When considering all the combinations of these 56 different products reacting only via (R2), (R3), and (R5) in Figure 1., the number of reactions becomes 17,220!

In order to make the calculations tractable while still retaining essential chemical information about this system, a "lumped" or "semi-detailed" approach is used to describe the oxidation chemistry. Similar approaches have been previously applied to kinetics modeling of gas-phase aerosol oxidation,[35] combustion,[36–39] and polymer chemistry.[29–31] Because of the symmetry of the molecule, squalane is broken up into a collection of hydrogen reactive sites as shown in Figure 3.. The concentration of each type of hydrogen is set to the initial concentration of squalane multiplied by the number of hydrogens for each type. The number of hydrogen sites used in the model corresponds to 6 tertiary hydrogens, 20 $\alpha$-secondary hydrogens (i.e. adjacent to a tertiary carbon center), 12 $\beta$-secondary hydrogens, and 24 primary hydrogens. After abstraction by OH, each type of reactive site, free radical intermediates, and reaction products is represented as separate functional group moieties. Thus, the transformation of squalane is considered as a collection of parallel reactions involving moieties representing the various parts of the molecule, with each site independent of the other sites. For simplicity hydrogen abstraction from primary sites and the resulting products are not included in any of the calculated reported here. Test models that include reactions at these sites predict very few functionalized products (<1%) since the reaction rate is slow.[40] The primary hydrogens are left in the model to keep track of their number, however. The concentrations of each of the hydrogen reactive site species used to initialize the model (along with other physiochemical properties) are shown in Table 1.Error: Reference source not found. This approach to constructing the reaction scheme enables the chemistry of functionalization for this system to be explored in a computationally efficient and physically meaningful way.

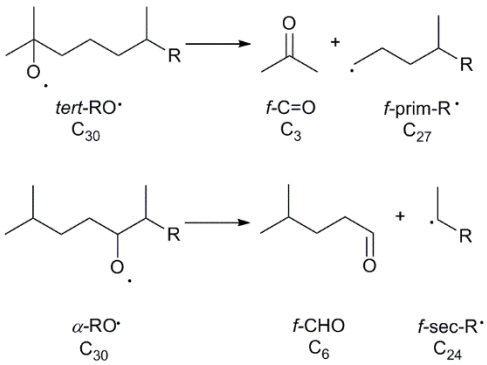


Figure 4. Two examples of alkoxy fragmentation reactions shown with the corresponding functional group, reactive intermediate, and carbon fragment marker species in the model. The prefix *f-* refers to a "fragment" functional group.

For fragmentation reactions, separate, independent carbon chain species are embedded as markers in each unimolecular dissociation step to track bond breaking in parallel with other chemical reactions. The model is initialized with a "$C_{30}$" species with a concentration equal to the initial concentration of squalane (see Table 1.). Upon fragmentation, the "$C_{30}$" species forms two smaller carbon fragments, such as "$C_3$" and "$C_{27}$". In addition to these carbon fragments, separate "fragment" functional group and reactive site species (denoted with "f" in Figure 4.) are also formed that continue to contribute to the chemistry. A couple of examples of how this chemistry is represented in the model are shown in Error: Reference source not found. All possible C-C bond breaking pathways are included, with each selected randomly as the simulation proceeds. In this way, the model can simulate both the number of carbon atoms and the carbon fragment distribution for comparison to experiment.

The simulation also calculates the aerosol particle volume using molecular densities as species are added or removed, enabling dynamic correction of concentrations of all species.[30] To initialize the calculation, the molecular volume of squalane (i.e. the inverse of density, $\rho_{Sq}$) is divided equally among the 30 different reactive sites. Then, as oxygen functional groups are added to the molecule or more volatile compounds are removed via evaporation, the volume of the particle is re-calculated to include changes due to additional functional groups or lost volatile species. As in Wilson et al.,[9] the density is assumed to start at 0.81 g cm$^{-3}$ (the density of squalane) and to increase by 0.03 g cm$^{-3}$ for each oxygen added weighted by its fraction of the whole

 

particle. The molecular density of the products of fragmentation reactions is defined in a similar fashion. A complete description of the calculation of the molecular density, along with a full list of the density of each species, is shown in the Supplementary Information in Table S-1. Using this variable-volume algorithm, the particle density and volume can be simulated as squalane is transformed through the mechanisms of functionalization and fragmentation.

By representing the heterogeneous reaction as a collection of hydrogen reactive sites, functional groups, and carbon fargments, the model predictions for average, measureable physiochemical properties (e.g. O/C ratio, carbon fragment distribution) can be compared with experiment. This model is a relatively compact, efficient model for the very complicated free radical chemistry. An example reaction scheme is included in the Supplementary Information (SI). Although a great deal of detail is included, the calculations are computationally inexpensive: a typical simulation time on a desktop computer is less than one second. While explicit information about the oxidative product generation is lost as a result of the semi-detailed description, this simplification allows the complex, multigenerational chemistry (over 10 oxidative lifetimes) of both functionalization and fragmentation.

### 2.2. Hydrogen abstraction and peroxy formation

The chemistry in the model begins with an OH abstraction of hydrogen from squalane, with a rate coefficient derived from the uptake coefficient of OH onto the squalane droplets from Smith et al.[24] The uptake coefficient $\gamma_{OH}$ is converted into a rate coefficient and then multiplied by the gas phase OH concentration, which is assumed to be constant, to give a pseudo-first order rate constant $k_{p\text{-}1st}$ for the hydrogen abstraction from squalane as shown below in Eq. (1).

$$k_{p\text{-}1st} = \frac{3\acute{c} M_{Sq} \gamma_{OH}}{2 d_p \rho_0 N_A} [OH(g)] \quad (1)$$

Here, $\acute{c}$ is the average molecular velocity of gas-phase OH at 298 K, $M_{Sq}$ is the molar mass of squalane (422 g/mol), $d_p$ is the mean surface weighted diameter of the squalane particles (160 nm) used in the experiment, $N_A$ is Avogadro's number, and $\rho_0$ is the particle phase density (0.81 g $cm^{-3}$). The extent of oxidation depends on OH exposure, which is the product of the OH concentration and reaction time,[24] so we compare the model predictions to experiment at different OH exposures (i.e. lifetimes). By setting the maximum simulation time to 78 seconds and keeping the OH concentration in the model constant, various OH exposures are obtained by examining the model output at different times. Using an average experimental concentration of OH of $10^{11}$ $cm^{-3}$, the overall reaction rate coefficient for abstraction of hydrogen used in the model is found to be $1.28 \times 10^{-1}$ $s^{-1}$. Using this rate coefficient, the model simulates a total OH exposure of $7.8 \times 10^{12}$ $cm^{-3}$ $s^{-1}$ in 78 seconds corresponding to approximately 10 squalane oxidation lifetimes.

While the average reactive uptake of OH onto squalane aerosol has been measured,[11,24] whether OH favors hydrogen abstraction at tertiary or secondary sites in the condensed phase remains unclear. The gas phase structure activity relationship (SAR) of Kwok and Atkinson[40] suggests that the abstraction of hydrogen from tertiary sites will be favored over secondary sites. In contrast, the SAR predictions for the aqueous phase hydrogen abstraction reactions by OH suggest that abstraction from neither tertiary nor secondary sites will be favored.[41,42] Given this difference in secondary and tertiary hydrogen reactivity, two different model assumptions based on these SAR predictions are compared. In one set of model scenarios (labeled "I"), abstraction of hydrogen from tertiary sites is assumed to be favored over abstraction from secondary sites as in the gas phase SAR. In another set of model scenarios (labeled "II"), abstraction from tertiary and secondary sites is equally probable as in the aqueous phase SAR. These rate coefficients are partitioned using statistical factors so that the overall rate coefficient for OH abstraction remains the same and is consistent with experiment. Thus, for example, under the model scenarios in which secondary and tertiary sites are equally probable, the rate coefficient for abstraction of tertiary hydrogens is $k_{tert} = 3k_{Sq}^{p\text{-}1st}/11$. In other words, 3 out of 11 OH abstraction reactions are from a tertiary site, and 8 out of 11 OH abstractions are from a secondary site. A list of each model assumption (including ones described later) is given in Table 2.. For a detailed list of the rate coefficients used with these model assumptions, see Table S-2 in the Supplementary Information.

The abstraction of hydrogen atoms by alkoxy radicals ((R6) in Figure 1.) is also considered in the model. Here, the bimolecular rate constant for hydrogen abstraction by alkoxy radicals is taken to be $1.66 \times 10^{-15}$ $cm^3$ $s^{-1}$ based on literature values for several different alkoxy abstraction reactions in the condensed phase.[21] The rate coefficient for abstraction for all alkoxy radicals is assumed to be the same. The reactions with each type of hydrogen reactive site are assumed to have the same relative probabilities as the OH abstraction reaction.

Table 2. Summary of different model assumptions about the chemical mechanism based on the chemistry of OH abstraction, the $RO_2$ self-reactions, and the fragmentation mechanism.

| Chemistry | Symbol | Description |
|---|---|---|
| OH abstraction | I | Abstraction from tertiary favored (based on gas phase SAR[40]) |
| OH abstraction | II | Neither tertiary nor secondary favored (based on aqueous SAR[41,42]) |
| $RO_2$ termination | A | 1 : 1 alcohol to ketone products (Russell products[17]) |
| $RO_2$ termination | B | Only ketone products (Bennett-Summers products[18]) |
| Secondary alkoxy | 1 | 10% of secondary $RO_2$ reactions |
| Secondary alkoxy | 2 | 5% of secondary $RO_2$ reactions |
| Alkoxy scission | a | Gas phase rate coefficient[16,43] |
| Alkoxy scission | b | Estimated condensed phase rate coefficient |
| Alkoxy scission | c | "Activated" scission from neighboring functional group |

After abstraction by either OH or alkoxy radicals, the resulting alkyl radicals reacts with oxygen to form peroxy radicals. Using the second order rate constant for oxygen addition to alkyl radicals in the condensed phase ($2.5 \times 10^{-12}$ $cm^3$ $s^{-1}$),[21] the gas phase concentration of $O_2$ in these experiments ($1.23 \times 10^{18}$ $cm^{-3}$),[24] and the Henry's law constant for oxygen and squalane ($K_{cc} = 0.18$),[44] the pseudo-first order rate coefficient for peroxy formation is found to be $5.54 \times 10^5$ $s^{-1}$. This value is used for the addition of $O_2$ to all alkyl radicals.

Once secondary alcohols form through functionalization reactions, the hydrogen atom on the same carbon as the alcohol is activated for abstraction by OH in both the gas[40] and aqueous[41,42] phase SAR. After reacting with $O_2$, the resulting hydroxyperoxy radicals are unstable and quickly decompose, forming a ketone and an $HO_2$ radical as shown in (R7).[45,46] The resulting $HO_2$ radicals could potentially react further with the $RO_2$ radicals, but since their reactions are relatively unknown in the condensed phase, no assumptions about the reactions of $HO_2$ radicals are included in any of the models shown here. Since the rate coefficient for the hydrogen abstraction from alcohols is so fast (see Table S-2), this reaction is included in all models.

$$R_2C(OH)OO^{\bullet} \rightarrow R_2C{=}O + HO_2^{\bullet} \qquad (R7)$$

Similarly, once fragmentation occurs, the resulting primary alcohols and aldehydes have hydrogen atoms that are highly activated toward OH abstraction. These reactions are thus also included in models that contain fragmentation chemistry. See Table S-2 in the Supplementary Information for the values of the rate constants for alcohol and aldehyde H-abstraction under each of the two SAR for OH abstraction.

### 2.3. Bimolecular reactions of peroxy radicals

After the abstraction of hydrogen and the addition of $O_2$, the resulting squalane peroxy radicals can react with another squalane peroxy radical to form alcohols, ketones, and alkoxy radicals as shown in (R1), (R2), and (R3) in Figure 1.. Rate coefficients for the $RO_2$ + $RO_2$ reaction are chosen based on a review of this reaction by Denisov and Afanasev.[21] For primary and secondary $RO_2$ radicals, the rate constants for the $RO_2$ + $RO_2$ reaction at 298 K are consistently around $1.61 \times 10^{-15}$ $cm^3$ $s^{-1}$. This rate coefficient is used for any reaction involving secondary alkyl peroxy radicals, including reactions with tertiary alkyl peroxy radicals. While some steric influence from the tertiary peroxy radical might slow this reaction, the available experimental rate coefficients for cross reactions between secondary and tertiary peroxy radicals[21,47] suggest that this steric effect is minor. For the $RO_2$ + $RO_2$ reaction between two tertiary peroxy radicals, the rate coefficient is somewhat lower than for reactions with secondary $RO_2$ radicals, however. Here, the rate coefficient is chosen to be $3.75 \times 10^{-16}$ $cm^3$ $s^{-1}$ based on the available experimental evidence; this value is likely an upper limit for the tertiary $RO_2$ self-reaction.[21]

While the reaction between two tertiary $RO_2$ radicals can only produce alkoxy radicals, the reactions involving primary or secondary $RO_2$ radicals can form alcohols, ketones, or alkoxy radicals as shown in Figure 1. and Figure 2.. Given that the branching ratios between each of these possible products of reactions involving secondary $RO_2$ radicals are unknown, several different assumptions about the reactivity of peroxy radicals are tested in different model scenarios. In the first set of model assumptions, the products in the radical termination reaction are set to only ketones as in (R1) in Figure 1. (i.e. Bennett-Summers products[18]) in model chemistry "B". For model chemistry "A", the products in the radical termination reaction are set to 1 : 1 alcohol to ketone as in (R2) in Figure 1. (i.e. "Russell" products[17]). These two model chemistries are chosen to reflect the extremes in possibilities – the actual branching ratio between ketones and alcohols in this reaction could also lie somewhere in between these two limiting cases. In the second set of model chemistries about secondary $RO_2$ reactions, the amount of secondary $RO_2$ that forms alkoxy radicals in the $RO_2$ + $RO_2$ reaction is also varied. Experimental estimates of the alkoxy branching ratio in the condensed phase are approximately 5-10%,[23] so the branching ratio to form alkoxy radicals is varied from 10% ("1") to 5% ("2"). These two sets of assumptions about the chemistry of secondary $RO_2$ radicals are used together in various model scenarios and compared with the experimental data to evaluate which functionalization mechanism is most consistent with experimental measurements. A subset of these model scenarios is then also used to test the fragmentation mechanisms in the oxidation of squalane.

In models that include fragmentation, acyl peroxy radicals ($R(O)OO^{\bullet}$) are formed by hydrogen abstraction from aldehydes and fragmentation of alkoxy radicals adjacent to ketones (see below). In both the gas[48–50] and condensed phase,[21,51] self-reactions of acyl peroxy radicals are relatively fast ($k = 5 \times 10^{-15}$ $cm^3$ $s^{-1}$ for the condensed phase) and yield acyloxy radicals that rapidly decompose to an alkyl radical and $CO_2$:

$$2\ RC(O)O_2^{\bullet} \rightarrow 2\ RC(O)O^{\bullet} + O_2 \rightarrow 2\ R^{\bullet} + 2\ CO_2 \quad (R8)$$

In the gas phase, the cross reactions of acyl peroxy with alkyl peroxy radicals are also relatively fast and yield either alkoxy and acyloxy radicals or a ketone and carboxylic acid.[48] However, since carboxylic acids are not observed as fragmentation products in the heterogeneous oxidation of squalane,[11] whether these same reactions apply to the liquid condensed phase remains unknown. Using the mechanism shown in Figure 2. as a guide to the condensed phase chemistry,[21,22] the following reactions are used in the model:

$$RC(O)O_2^{\bullet} + RO_2^{\bullet} \rightarrow RC(O)O^{\bullet} + RO^{\bullet} + O_2 \quad (R9a)$$

$$RC(O)O^{\bullet} + R_2C{=}O + HO_2^{\bullet} \quad (R9b)$$

The rate coefficient for this reaction is assumed to be the same as that for the associated $RO_2$ radical. Both of the pathways are assumed to be equally likely for secondary $RO_2$ radicals, with only (R9a) possible for tertiary $RO_2$ radicals. $RC(O)O^{\bullet}$ is assumed to rapidly decompose into $CO_2$ and an alkyl radical as in (R8). Other possible branching ratios or products could occur in these reactions in the condensed phase. Since these reactions only start to become important at much later stages in the oxidation, the exact assumptions about these reactions do not have a large effect on the simulation results.

### 2.4. Alkoxy Decomposition

The $\beta$-scission of alkoxy radicals is the primary fragmentation mechanism considered in the model. However, even in the gas phase, only a few of the rate constants for decomposition of alkoxy radicals have been measured.[16] To reflect this experimental uncertainty, several different model assumptions about alkoxy scission are used. A summary is given in Table 2.. Under the model assumption "a", gas phase rate coefficients for structurally similar alkoxy radicals are used for the scission of the secondary and tertiary alkoxy radicals. The rate coefficients do not seem to vary much between structurally similar alkoxy radicals. For example, 2-methyl-2-butoxyl and 2-methyl-2-pentoxyl radicals have gas phase decomposition rate coefficients of $\sim 1.5 \times 10^4$ s$^{-1}$ at 298 K.[16,52] As such, since the tertiary alkoxy radical of squalane is structurally similar to those smaller alkoxy radicals, this same rate coefficient is used in the model. Similarly, the rate coefficients for decomposition of structurally similar secondary alkoxy radicals[16,43] are used for the decomposition of $\alpha$- and $\beta$-secondary alkoxy radicals. For decomposition of the tertiary, $\alpha$-secondary, and $\beta$-secondary alkoxy radicals to form a primary radical, the values of the rate coefficients are taken to be $1.5 \times 10^4$ s$^{-1}$. For the decomposition of an $\alpha$-secondary alkoxy radical to a secondary radical, the value of the rate coefficient is taken to be $3.5 \times 10^4$.

The possible effect of solvation on the alkoxy decomposition rate coefficients is also tested in a second model assumption (labeled "b"). The limited number of experimental measurements of decomposition rate coefficients of alkoxy radicals in aqueous solution suggest that the rate for decomposition is enhanced in the condensed phase compared to the gas phase.[53] However, to what extent the rate coefficient is enhanced in the organic condensed phase compared to the gas phase is currently unknown. As such, electronic structure calculations (see the Supplementary Information (SI) for details) are used to estimate the change in barrier height for alkoxy scission in the condensed phase. Based on these calculations, the barrier height decreases by ~0.8 kcal mol$^{-1}$ from the gas phase independent of the molecular structure used. Using the value for $A_{TST}$ recommended in Vereecken and Peeters,[43] this reduction in barrier height leads to rate coefficients for decomposition of alkoxy radicals that are five times faster at 298 K in model assumption "b".

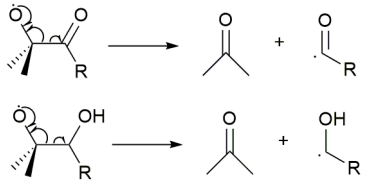


Figure 5. Two examples of "activated" alkoxy decomposition, where the presence of a functional group on the adjacent carbon reduces the barrier height to decomposition.

In the third assumption for alkoxy radical decomposition, the presence of functional groups on adjacent carbon atoms is tracked in the model since the barrier height to alkoxy decomposition is significantly reduced for these types of radicals (see Error: Reference source not found).[16,43] For an alkoxy radical with a hydroxyl or carbonyl functional group located on the $\beta$-carbon, the barrier height to decomposition is reduced from approximately 12 kcal mol$^{-1}$ to approximately 6 kcal mol$^{-1}$, based on the limited experimental measurements available[16] and electronic structure calculations.[43] This reduction in barrier height for alkoxy decomposition alters the competition between hydrogen abstraction (R5) and decomposition (R6) in Figure 1. so that decomposition (R6) dominates over hydrogen abstraction (R5) for alkoxy radicals with an adjacent functional group. This chemistry becomes particularly important at later stages of the reaction after the aerosol has become more oxidized.

To include the possibility that an alkoxy radical is formed at a site adjacent to an existing functional group, the neighboring hydrogen atom sites are converted into an "activated" hydrogen site in model assumption "c". These activated hydrogen sites have chemistry otherwise identical to their parent hydrogen sites (e.g. tertiary hydrogen), except that their alkoxy decomposition rate coefficients are increased from $\sim 10^4$ s$^{-1}$ to $\sim 10^9$ s$^{-1}$ to account for the decrease in the barrier height. The resulting ketyl and acyl radicals formed via these "activated" fragmentation reactions react via (R7), (R8), and (R9) to give aldehydes and additional alkyl fragment radicals.

### 2.5. Evaporation

Accurate model predictions of the changes in aerosol volume and mass observed in the experiment requires

evaporation of the smaller molecular weight reaction products from the aerosol to be considered in some detail. For the carbon fragments formed from alkoxy scission, their evaporation is considered as the irreversible thermal desorption from the surface of the particle. Since the particle is considered instantaneously mixed, diffusion to the surface of the particle is not considered here although it may matter for semisolid or solid particles. The gas phase species produced by evaporation are assumed not to contribute further to the chemistry as they are assumed to not re-adsorb onto the surface of the droplet.

The rate coefficient for the evaporation of carbon fragments ($k_{evap}$) is calculated from the vapor pressure ($p_{vap}$) estimated from SIMPOL.1,[54] the desorption flux from the Hertz-Knudsen equation, the surface area of the particle, and Raoult's Law. First, the vapor pressure of each carbon fragment is estimated using SIMPOL.1[54] by assuming only one alcohol, ketone, or aldehyde functional group per carbon fragment. Then, the desorption flux is calculated from this vapor pressure using the Hertz-Knudsen equation for adsorption and microscopic reversibility:

$$J_{\mathrm{des}} = \frac{\alpha\, p_{\mathrm{vap}}}{\sqrt{2\pi mkT}} \quad (2)$$

Here, $m$ is the molecular mass, $k$ is Boltzmann's constant, $T$ is the temperature, and $\alpha$ is the accommodation coefficient for the fragment at the surface, which is assumed to be 1. To change the desorption flux into a molecular rate for the loss of species C from thermal desorption, both sides of Eq. (2) are multiplied by the surface area of the particle (in terms of the particle diameter $d_p$) to give Eq. (3).

$$\frac{d[\mathrm{C}]}{dt} = -\alpha\, d_p^2\, p_{\mathrm{vap}} \sqrt{\frac{\pi}{2\,mkT}} \quad (3)$$

Since this expression only gives the evaporation rate from a particle of pure component C, the vapor pressure is multiplied by the number fraction of component C as in Raoult's law. The number fraction of C is approximated by assuming that the total number density of molecules is the same as the initial molecular concentration of squalane ($[\mathrm{Sq}]_0 = 1.15 \times 10^{21}$ cm$^{-3}$), yielding the following equations for the rate of loss of carbon fragment C and by analogy the rate coefficient for thermal desorption $k_{evap}$:

$$\frac{d[\mathrm{C}]}{dt} \approx -\frac{\alpha\, d_p^2\, p_{\mathrm{vap}}}{[\mathrm{Sq}]_0} \sqrt{\frac{\pi}{2\,mkT}} [\mathrm{C}] \quad (4)$$

$$k_{\mathrm{evap}} \approx \frac{\alpha\, d_p^2\, p_{\mathrm{vap}}}{[\mathrm{Sq}]_0} \sqrt{\frac{\pi}{2\,mkT}} \quad (5)$$

In practice, the estimated evaporation rate coefficient has to be lowered by a factor of 10 (see SI) to predict the correct experimental carbon fragment distribution;[11] thus, it is one of the only adjustable parameters in the model. This reduction in the evaporation rate coefficient likely captures the effect of non-ideal deviations from Raoult's Law and the relative errors in the vapor pressures estimated from SIMPOL.1, since the SIMPOL.1 SAR tends to over-predict the vapor pressures of alcohols and aldehydes by 50%.[54] In addition, this might also potentially indicate an accommodation coefficient less than 1, although we cannot determine a value of $\alpha$ with this model. A list of the vapor pressures and rate coefficients for evaporation is given in Table S-3 in the Supplementary Information.

## 3. Simulation Results

Because of the many unknowns regarding the molecular details of the oxidation of squalane, in particular regarding peroxy and alkoxy radicals, several sets of different model scenarios are considered that explore different assumptions about the reactivity of squalane, its radical intermediates, and its reaction products. The various assumptions are combined in each model scenario and are used to explore the functionalization and fragmentation mechanisms most consistent with the measured chemical and physical properties of the aerosol after oxidation. These different assumptions and their associated chemistry are summarized in Table 2.. For example, the model scenario labeled "I-B-2"describes a model in which abstraction of tertiary hydrogens is favored, only ketones are formed from the $RO_2$ + $RO_2$ termination reaction involving secondary $RO_2$, and secondary alkoxy radicals form 5% of the time in an $RO_2$ + $RO_2$ reaction. Each possible combination of different assumptions about the chemistry was tested in the model, but for clarity, only a subset of those model scenarios are shown here. These model scenarios are compared with experiment to find the mechanisms most consistent with the available experimental data on the heterogeneous oxidation of squalane.

To compare the model results with experiment, the various species are converted from concentrations into numbers of carbon, hydrogen, and oxygen atoms by multiplying by the volume and stoichiometry. The number of each type of atoms is then used to calculate the mass, density, H/C, and O/C ratios of the droplet. These values are then compared to the experimentally measured values reported in Kroll et al.,[10] which are re-evaluated to correct the elemental ratios for loss of CO and $H_2O$ in the AMS.[55] For the functionalization models, the H/C and O/C are compared to experiment using the slope in a "Van Krevelen plot". As discussed previously,[3,56] a slope in this type of plot can describe the average evolution of different functional groups within the aerosol as it becomes more oxidized. By comparing simulations with the experimental slope on a Van Krevelen plot, we can evaluate which functionalization mechanisms are most consistent with the experimental results. Fragmentation mechanisms are then added to this subset of of the functionalization models and are compared with the experimental measurements of aerosol mass, density, volume, average molecular formula, and carbon fragment distribution over ten oxidation lifetimes.

### 3.1. Functionalization mechanism comparison

 

The functionalization models can be compared with experiment to see which mechanisms are most consistent with the evolution of functional groups in the aerosol. Using the corrected O/C data from Kroll et al.,[10] the initial slope on the Van Krevelin plot is -1.77 until an O/C ratio of approximately 0.15, consistent with ketones being the primary reaction product. At this point, the slope changes to -0.79, which is more consistent with a combination of alcohols and ketones (or carboxylic acids). Overall, the plot exhibits a slope of -1.17 over 10 lifetimes. The newly corrected experimental data, along with different model scenarios, are shown in Figure 6.A.

By comparing the different model scenarios shown in Figure 6. with experiment, several aspects of the mechanism become apparent. The initial abstraction of hydrogen has a strong influence on the distribution of functional groups within the aerosol. For example, model scenarios using "I" in which hydrogen abstraction from tertiary sites is favored over secondary sites as in the gas phase SAR,[40] the slopes in Figure 6.A are approximately -0.8, which indicates that alcohols are generally favored over ketones. The formation of alcohols is favored because the lack of $\alpha$-hydrogen on the resulting tertiary $RO_2$ radicals promotes the formation of alkoxy radicals through (R9) or blocks the formation of a second ketone via (R10). Examining the ratio of alcohol : carbonyl products in Figure 6.B can provide further insight into the underlying product distribution that controls this slope. In this case, the ratio of products develops dynamically with the O/C ratio so that initially alcohol products are highly favored but become less favored as the aerosol becomes oxidized. In contrast, model scenarios using "II" in which hydrogen abstraction from tertiary sites has the same rate as from secondary sites,[41,42] and the slope is less than -1, indicating that ketones are more favored over alcohols. In this case, the alcohol : carbonyl ratio remains mostly constant as the O/C ratio increases.

Other assumptions about the chemical mechanism of aerosol oxidation can also affect the slope and product ratios, although not to the same extent as the chemistry of the initial OH abstraction. The branching ratios for the products of the reaction between two secondary $RO_2$ radicals also influences the slope in Figure 6., particularly when hydrogen abstraction from tertiary sites is not favored. As might be expected, exclusive formation of ketones (i.e. "B") in the secondary $RO_2$ termination reaction decreases the slope and the alcohol : carbonyl ratio, as shown in Figure 6.. In contrast, the branching ratio for alkoxy formation from secondary $RO_2$ radicals has a small influence on the slope. A comparison of II-B-1 and II-B-2 shows that the slope on the Van Krevelen plot only slightly decreases when the alkoxy radical formation branching ratio is decreased from 10% to 5%. Notably, including mechanisms for alkoxy fragmentation (as in scenario II-B-1-bc) also does not have a strong effect on the slope and the alcohol : carbonyl product ratio.

Of the possible mechanisms for functionalization, model scenario II-B-1 is most consistent with experiment, suggesting that termination reactions with secondary $RO_2$ radicals might indeed favor ketones in the condensed phase, consistent with the experimental observations of Hearn et al.[20] However, model scenario I-B-1 is also possible within the experimental error of the measurement. The site preference of the initial OH abstraction has the strongest influence on the Van Krevelen plot and the alcohol : carbonyl ratio with the termination products of secondary $RO_2$ reactions only playing a minor role. In contrast, the alkoxy radical formation branching ratio for secondary $RO_2$ radicals and the fragmentation of alkoxy radicals both only have a minor effect on both the slope and the alcohol : carbonyl ratio predicted by the model.

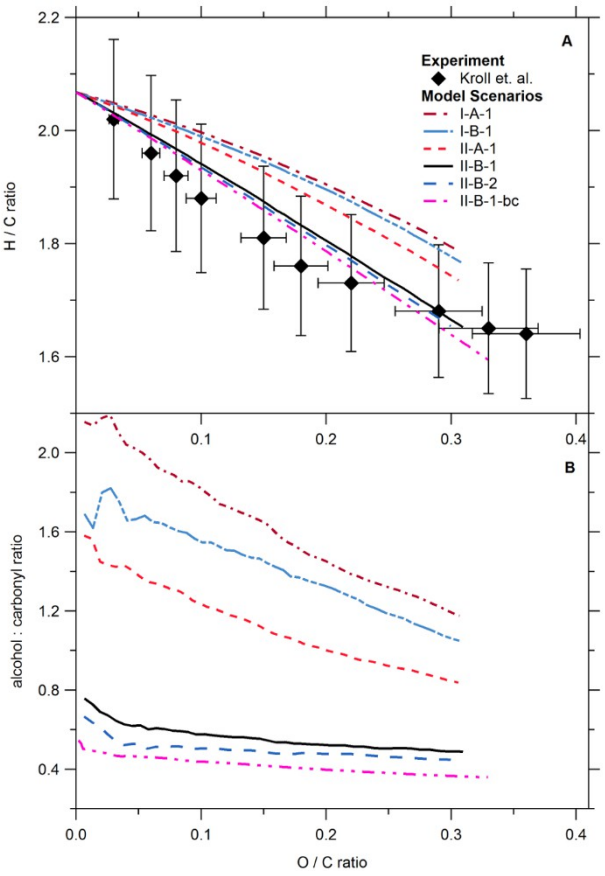


Figure 6. (**A**) Van Krevelin plot comparing the experimental data from Kroll et al.[10] to various model scenarios. Each letter or numeral refers to a specific type of chemistry in the model (described in Table 2.). For example, "I" or "II" refer to different hydrogen abstraction rate coefficients for hydroxyl radicals, and A", "B", "1", and "2" refer to different branching ratios for the chemistry of secondary $RO_2$ radicals. See sections 2.2, Error: Reference source not found, and Table 2. for more details about the chemistry used in these scenarios. (**B**) Change in the ratio of alcohol functional groups to carbonyl functional groups in the model with increasing O/C ratio. Note that the noise at low O/C ratio is due to statistical variation from the stochastic simulation method.

### 3.2. Fragmentation mechanism comparison

To completely describe the evolution of aerosol oxidation, fragmentation mechanisms need to be included in the model In the experiment,[10] the measured mass and the

number of oxygen atoms initially increases due to oxidation, the number of hydrogen atoms decreases, and the volume and number of carbon atoms remain the same, consistent with functionalization dominating at the early stages of the reaction. After approximately two oxidation lifetimes, the volume, mass, and number of carbon atoms start to decrease while the number of oxygen atoms continues to increase, which indicates the increasing importance of fragmentation reactions. Finally, near seven oxidation lifetimes, the number of oxygen atoms stops increasing while the volume, mass, and number of carbon atoms continue to decrease as fragmentation dominates.

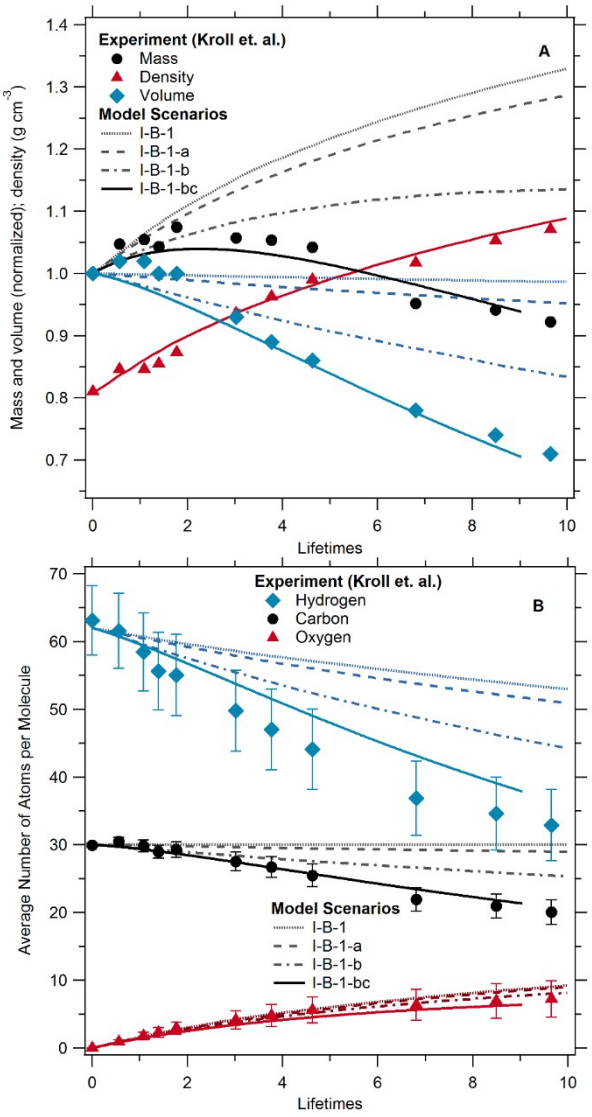


Figure 7. Comparison of the measured mass, volume, density, and chemical composition of the aerosol with the model predictions when various fragmentation mechanisms are included in the chemical mechanism. For these model scenarios, abstraction from tertiary sites is assumed to be favored (i.e. assumption "I", see Table 2.). For the fragmentation mechanisms, "a" refers to gas-phase alkoxy decomposition rate coefficients, "b" refers to the estimated condensed phase alkoxy decomposition rate coefficients, and "c" refers to activated alkoxy decomposition in which an adjacent oxygen functional group greatly increases the decomposition rate coefficient. Note that the density does not change appreciably between different model scenarios.

To explore the underlying mechanisms of C-C bond scission (i.e. fragmentation), the model predictions of aerosol mass, volume, the average number of carbon, oxygen, and hydrogen atoms, and the carbon number distribution of products can be compared with experiments.[10,11] Since the model scenarios I-B-1 and II-B-1 are most consistent with the Van Krevelen plots, these scenarios are used as a functionalization "baseline" for subsequent models that include fragmentation. Other model scenarios that are not shown were also tested with different combinations of the assumptions listed in Table 2., but they were unable to accurately predict the experimental data as well as the two described above.

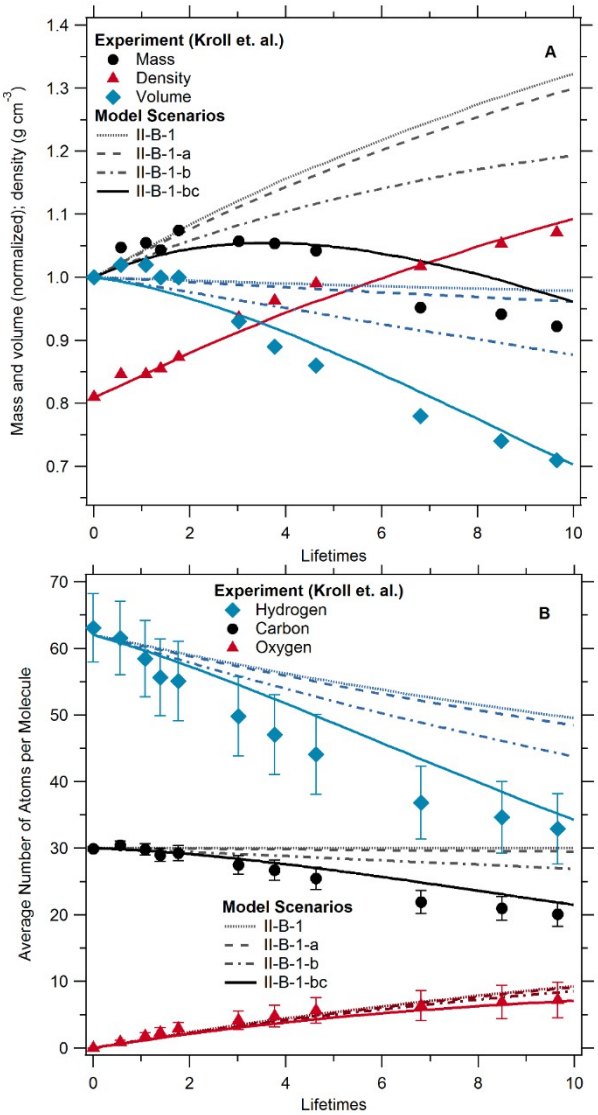


Figure 8. Same as Figure 7., except abstraction from neither tertiary nor secondary sites is assumed to be favored (i.e. assumption "II", see Table 2.).

The change in the physical and chemical properties of the aerosol under model assumptions “a” (i.e. gas phase decomposition), “b” (i.e. estimated condensed phase decomposition), and “b” combined with “c” (i.e. “activated” decomposition) can be seen in Figure 7. and Figure 8.. As alkoxy decomposition becomes more facile going from model assumption “a” (gas phase alkoxy decomposition) to “bc” (“activated” alkoxy decomposition), more mass, volume, hydrogen, and carbon loss are predicted by the model. Of the various model scenarios shown on Figure 7. and Figure 8., the scenarios I-B-1-bc and II-B-1-bc (shown as solid lines) are most consistent with the experimental physical and chemical properties of the aerosol. In both cases, the “activated” alkoxy decomposition from neighboring functional groups must be included in the model in order to correctly predict the chemical and physical properties after 5 lifetimes.

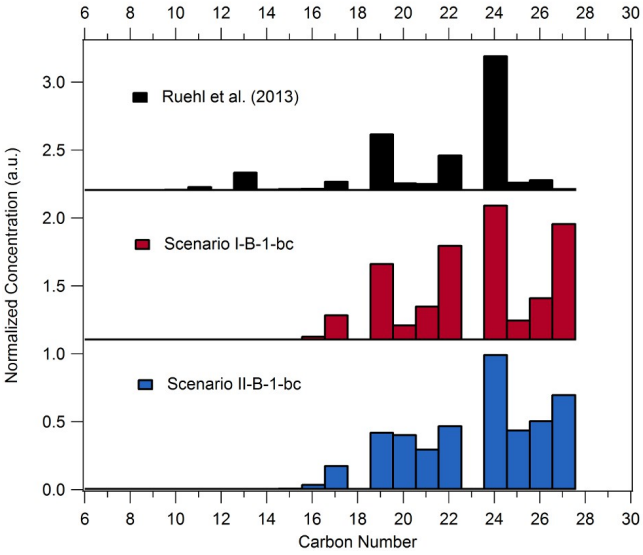


Figure 9. Concentration of fragmentation products versus carbon number in experiment and two model scenarios. Both the experiment and the model results are normalized to the largest peak in the carbon number distribution of products. The carbon number distribution of products from Ruehl et al.[11] and two model scenarios that included of “activated” alkoxy decomposition are shown at ~0.9 lifetimes. The two model scenarios use different assumptions about the OH abstraction probabilities.

For the two model scenarios most consistent with the measured mass, volume, and elemental losses, the simulations are compared to the carbon number distribution of fragmentation products from Ruehl et al.[11] The experimental carbon number distribution at ~0.9 lifetimes consists of stable ketone, aldehyde, and alcohol products from fragmentation measured using two dimensional gas chromatography that separates compounds by polarity and volatility. The data indicates that most of the fragmentation products are formed adjacent to tertiary sites. However, since analytical standards for these fragmentation products are not available, only a qualitative comparison of the experiment and model is currently possible. Despite this limitation, model-measurement comparison provides a further experimental constraint on possible fragmentation mechanisms.

In Figure 9., the differences between a model scenario in which abstraction from tertiary sites is favored (i.e. “I”) and a model in which abstraction from secondary and tertiary sites has the same rate (i.e. “II”) are compared. Based on a comparison with experiment, the scenario I-B-1-bc best predicts the carbon number distribution of fragmentation products. However, both model scenarios predict a somewhat large peak for C27 aldehyde that was not observed experimentally. In the original experiment, the C27 aldehyde likely co-elutes with the large, broad squalane peak in the GC x GC columns so that it was not observed. Furthermore, the rate coefficient for alkoxy decomposition to form C27 products is unlikely to be drastically different than rate coefficients for similar reactions to form aldehydes with similar structures, such as the C22 or C17 aldehydes. Small peaks corresponding to C11 and C13 products are observed experimentally but are not predicted by the model because they desorb quickly and therefore are not predicted to be present for GC x GC analysis. The evaporation rate coefficients for these products may be too large in the model because of non-ideal deviations from Raoult’s Law, although the source of this variance is somewhat unclear. Simulations that incorporate diffusion may help to improve our understanding of the evaporation processes and explain the differences between calculations and experiments. Nonetheless, based on the carbon number distribution and the changes in the mass, volume, and elemental composition in Figure 7. and Figure 8., model scenario I-B-1-bc is the most consistent with the global experimental data set.

## 4. Discussion

Using stochastic simulation methods and a semi-detailed approach to the kinetics, the mechanisms of functionalization and fragmentation in the heterogeneous oxidation of well-mixed organic aerosol by gas-phase OH radicals can be represented as a conversion between various hydrogen, oxygen, and carbon functional groups. The time history of total mass, volume, density, hydrogen, oxygen, and carbon content, and the carbon fragment distribution can be predicted using realistic representations of free radical reaction pathways and published rate coefficients from the literature. The stochastic algorithms used here allow for a flexible yet quantitative representation of the chemistry that typically would not be possible with integrated differential equations. Furthermore, the algorithm allows the volume to vary over the entire calculated time history, dynamically altering the concentrations as the oxidation proceeds. This approach to representing the chemistry allows for a realistic description of the underlying mechanisms of functionalization and fragmentation in the heterogeneous oxidation of organic aerosol despite the significant complexity of the chemistry.

The functionalization chemistry is driven primarily by the site preference of the initial OH abstraction with the product branching ratio for secondary $RO_2$ radicals also

playing a minor role, as shown on Figure 6.. In contrast, when OH has no site preference for tertiary or secondary hydrogen, more ketone products are formed since secondary $RO_2$ can form all three possible products from $RO_2$ chemistry shown in Figure 1..

The fragmentation chemistry, is driven by the decomposition of "activated" alkoxy radicals, in which a functional group is located on the $\beta$-carbon to the alkoxy group. As oxygen is added to the aerosol over time, more oxidized aerosol undergoes more fragmentation, as has been noted previously.[5,9,10,12,24,56–58] Here, however, a molecular mechanism for why more fragmentation occurs in oxidized aerosol is revealed explicitly by examining the fraction of OH abstraction reactions that lead to fragmentation as shown in Figure 10.. In the initial stages of oxidation, the only pathway for fragmentation is through decomposition of alkyl alkoxy radicals — a slow reaction that occurs at a rate of only ~2% relative to the rate of OH abstraction. As more functional groups are added to the organic aerosol, though, the probability that an alkoxy radical is formed on the carbon $\beta$ to a functional group increases as O/C increases, enhancing the frequency of "activated" alkoxy fragmentation reactions. Because of the reduction in the barrier height to decomposition, 99% of alkoxy radicals formed adjacent to functional groups decompose to give smaller carbon number products. Notably, the products from these activated decomposition reactions not only promote further free radical chemistry but also can fragment themselves to produce even smaller carbon fragments (e.g. through R8).

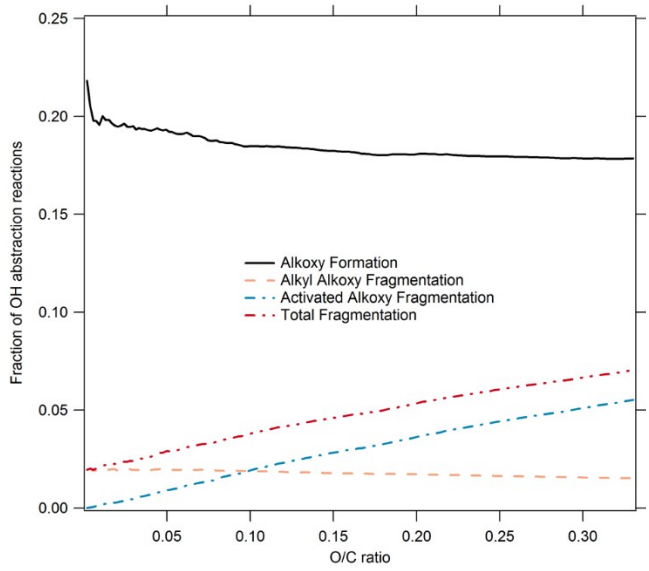


Figure 10. Fraction of OH abstraction reactions that lead to alkoxy formation and alkoxy fragmentation as a function of the O/C ratio in model scenario I-B-1-bc.

Other factors can also influence the alkoxy decomposition reaction as the O/C ratio increases. For example, previous measurements have shown that the rate coefficient for decomposition of *tert*-butoxy radicals is enhanced by nearly four orders of magnitude in the aqueous phase over the gas phase.[21,53] Similarly, the barrier height for alkoxy decomposition in electronic structure calculations using 5-nonanone as a solvent instead of n-hexdecane (see SI) show a decrease in barrier height from the gas phase of about 2 kcal $mol^{-1}$. These observations suggest that factors such as polarity could increase the decomposition rate coefficients for alkoxy radicals even further as O/C increases as the aerosol becomes more oxidized.

Although these other factors might influence the decomposition of alkoxy radicals, the "activated" alkoxy decomposition may be the dominant mechanism for fragmentation in aerosol.[57,58] For more oxidized aerosol, the alkoxy decomposition would likely dominate over hydrogen abstraction or other reactions, since all alkoxy radicals formed would be adjacent to a functional group. Furthermore, "activated" alkoxy decomposition provides an underlying molecular mechanism for the empirical fragmentation operator presented in Wilson et al.[9] for squalane and bis(2-ethylhexyl)sebacate.

While the model predicts the physical and chemical properties of the aerosol over 10 lifetimes, several key uncertainties exist, particularly in regard to the initial hydrogen abstraction by OH. Neither the functionalization nor fragmentation models provided unambiguous evidence for whether abstraction of hydrogen at an organic surface from the tertiary sites is favored as in the gas phase (i.e. "I")[40] or whether abstraction of hydrogen from secondary and tertiary sites is equally favored as in the aqueous phase (i.e. "II").[41,42] For example, the Van Krevelen plot in Figure 6. suggests that abstraction from tertiary and secondary sites are equally favored, but the comparison with the experimental carbon number distribution in Figure 9. suggests that abstraction from tertiary sites is favored. In fact, since we are considering a case that is neither bulk nor gas phase (i.e. an interface), that the site preference for OH abstraction is different from the predictions of these two SAR is not surprising. Some experimental uncertainties also remain in the measurements of the O/C and H/C ratio[10] since they were developed for ambient organic aerosol,[55,59] which makes discerning differences between model scenarios difficult. Furthermore, as discussed earlier, quantitative comparisons of the model and experimental carbon fragment distribution from Ruehl et al.[11] are difficult because of a lack of analytical standards for fragmentation products.

Another uncertainty in the model chemistry is the branching ratio for formation of secondary alkoxy radicals. Although a branching ratio of 10% for formation of alkoxy radicals from all secondary peroxy radicals (including "activated" alkoxy radicals) is found to best predict the experimental results, the combination of assumptions used with this branching ratio could have led to a fortuitous prediction. For secondary alkoxy radicals, differences in structure or nearby functional groups could lead to different branching ratios. For example, previous experimental work[23] suggests that nearby functional groups assist in the formation of alkoxy radicals within the radical cage, leading to a greater branching ratio than simple alkoxy radicals. An

increase in this branching ratio would lead to increased fragmentation, so that other rate coefficients, such as those for the decomposition of alkyl alkoxy radicals, would have to decrease to compensate.

Given the importance of alkoxy radical decomposition to understanding the chemistry of fragmentation for organic aerosol aging, additional measurements of decomposition rate coefficients for alkoxy radicals are necessary. Currently, only a paucity of measurements in the gas phase[16] and condensed phase[21] are available. Furthermore, current SAR[16,43] for this reaction do not adequately predict the experimental barrier heights and rate coefficients because few measurements exist. As such, additional measurements with a variety of structures and functional group substitutions and in the gas phase and different solvents could help resolve much of the uncertainty regarding the fragmentation mechanism.

## 5. Conclusions

Using a stochastic simulation method to model the kinetics as conversions of hydrogens at different reactive sites to different functional groups, many different measured average chemical and physical properties of squalane aerosol can be predicted as it is oxidized by gas phase OH radicals. Using this model, a molecular description of the mechanisms of functionalization and fragmentation of aerosol oxidation is developed by testing different model assumptions about the underlying chemical mechanism. For functionalization, the site preference of the initial OH abstraction from the aerosol is found to primarily control the resulting functional group distribution, with the branching ratio between different products in the secondary $RO_2$ self-reactions also playing a role. For fragmentation, the decomposition of activated alkoxy radicals in which a functional group is located on the $\beta$-carbon is found to drive the fragmentation of organic aerosol as the O/C ratio increases. Some aspects of the underlying chemistry in oxidation remain ambiguous, but additional measurements, particularly of the decomposition rate coefficients for alkoxy radicals in the condensed phase, could help improve this model and test the validity of some the underlying assumptions. Regardless, this scheme helps connect the measurable average aerosol properties to the underlying mechanisms of free radical chemistry in aerosol oxidation.

The kinetic scheme developed here to investigate the chemical mechanism of oxidation of squalane aerosol could also be extended to describe other model aerosol oxidation systems. Extensions would involve adding reaction steps for new moieties containing functionalities such as double bonds and aromatic rings, and expanding oxidant types to include other initiation processes besides H abstraction. This framework could be used directly to understand the oxidation mechanisms and could be compared with more parameterized approaches to test their validity. As experimental data become available other conditions such as higher or lower temperature can be investigated with this model. By applying the scheme developed here to other model systems and to less well-mixed semisolid or glassy aerosol, the chemical mechanisms can be investigated to better constrain the evolution of more complex organic aerosol in the atmosphere and provide a molecular understanding of the underlying processes.

### Acknowledgements

This material is based upon work supported by the Laboratory Directed Research and Development Program of the Department of Energy's Lawrence Berkeley National Laboratory under U.S. Department of Energy Office of Science, Office of Basic Energy Sciences under Contract No. DE-AC02-05CH11231. Results were used from past K.R.W. work supported by the Department of Energy's Office of Science Early Career Research Program and by Chemical Sciences Division of the U.S. Department of Energy under Contract No. DE-AC02-05CH11231. W.D.H. is supported by CHTC. Special thanks to B. Kirk for help with electronic structure calculations.

## 6. Notes and references

[a] Chemical Sciences Division, Lawrence Berkeley National Laboratory, Berkeley, CA 94720, USA.

[b] Columbia Hill Technical Consulting, Fremont, CA 94539, USA.

*First corresponding author: fahoule@lbl.gov

Second corresponding author: krwilson@lbl.gov

Electronic Supplementary Information (ESI) available: [details of any supplementary information available should be included here]. See DOI: 10.1039/b000000x/

1. A. H. Goldstein and I. E. Galbally, *Environ. Sci. Technol.*, 2007, **41**, 1514–1521.
2. N. M. Donahue, S. a. Epstein, S. N. Pandis, and a. L. Robinson, *Atmos. Chem. Phys.*, 2011, **11**, 3303–3318.
3. C. L. Heald, J. H. Kroll, J. L. Jimenez, K. S. Docherty, P. F. DeCarlo, a. C. Aiken, Q. Chen, S. T. Martin, D. K. Farmer, and P. Artaxo, *Geophys. Res. Lett.*, 2010, **37**, n/a–n/a.
4. J. L. Jimenez, M. R. Canagaratna, N. M. Donahue, a S. H. Prevot, Q. Zhang, J. H. Kroll, P. F. DeCarlo, J. D. Allan, H. Coe, N. L. Ng, a C. Aiken, K. S. Docherty, I. M. Ulbrich, a P. Grieshop, a L. Robinson, J. Duplissy, J. D. Smith, K. R. Wilson, V. a Lanz, C. Hueglin, Y. L. Sun, J. Tian, A. Laaksonen, T. Raatikainen, J. Rautiainen, P. Vaattovaara, M. Ehn, M. Kulmala, J. M. Tomlinson, D. R. Collins, M. J. Cubison, E. J. Dunlea, J. a Huffman, T. B. Onasch, M. R. Alfarra, P. I. Williams, K. Bower, Y. Kondo, J. Schneider, F. Drewnick, S. Borrmann, S. Weimer, K. Demerjian, D. Salcedo, L. Cottrell, R. Griffin, A. Takami, T. Miyoshi, S. Hatakeyama, A. Shimono, J. Y. Sun, Y. M. Zhang, K. Dzepina, J. R. Kimmel, D. Sueper, J. T. Jayne, S. C. Herndon, a M. Trimborn, L. R. Williams, E. C. Wood, a M. Middlebrook, C. E. Kolb, U. Baltensperger, and D. R. Worsnop, *Science*, 2009, **326**, 1525–9.
5. J. H. Kroll, N. M. Donahue, J. L. Jimenez, S. H. Kessler, M. R. Canagaratna, K. R. Wilson, K. E. Altieri, L. R. Mazzoleni, A. S. Wozniak, H. Bluhm, E. R. Mysak, J. D. Smith, C. E. Kolb, and D. R. Worsnop, *Nat. Chem.*, 2011, **3**, 133–9.
6. J. F. Pankow and K. C. Barsanti, *Atmos. Environ.*, 2009, **43**, 2829–2835.
7. N. M. Donahue, a L. Robinson, C. O. Stanier, and S. N. Pandis, *Environ. Sci. Technol.*, 2006, **40**, 2635–43.

8. N. L. Ng, M. R. Canagaratna, Q. Zhang, J. L. Jimenez, J. Tian, I. M. Ulbrich, J. H. Kroll, K. S. Docherty, P. S. Chhabra, R. Bahreini, S. M. Murphy, J. H. Seinfeld, L. Hildebrandt, N. M. Donahue, P. F. DeCarlo, V. A. Lanz, A. S. H. Prévôt, E. Dinar, Y. Rudich, and D. R. Worsnop, *Atmos. Chem. Phys.*, 2010, **10**, 4625–4641.
9. K. R. Wilson, J. D. Smith, S. H. Kessler, and J. H. Kroll, *Phys. Chem. Chem. Phys.*, 2012, **14**, 1468–79.
10. J. H. Kroll, J. D. Smith, D. L. Che, S. H. Kessler, D. R. Worsnop, and K. R. Wilson, *Phys. Chem. Chem. Phys.*, 2009, **11**, 7759.
11. C. R. Ruehl, T. Nah, G. Isaacman, D. R. Worton, A. W. H. Chan, K. R. Kolesar, C. D. Cappa, A. H. Goldstein, and K. R. Wilson, *J. Phys. Chem. A*, 2013, **117**, 3990–4000.
12. C. W. Harmon, C. R. Ruehl, C. D. Cappa, and K. R. Wilson, *Phys. Chem. Chem. Phys.*, 2013, **15**, 9679–93.
13. J. J. Orlando and G. S. Tyndall, *Chem. Soc. Rev.*, 2012, **41**, 6294–317.
14. R. Atkinson and J. Arey, *Chem. Rev.*, 2003, **103**, 4605–38.
15. G. S. Tyndall, R. A. Cox, C. Granier, R. Lesclaux, G. K. Moortgat, M. J. Pilling, A. R. Ravishankara, and T. J. Wallington, *J. Geophys. Res. Atmos.*, 2001, **106**, 12157–12182.
16. R. Atkinson, *Atmos. Environ.*, 2007, **41**, 8468–8485.
17. G. A. Russell and B. Y. Glen, *J. Am. Chem. Soc.*, 1957, **79**, 3871–3877.
18. J. E. Bennett and R. Summers, *Can. J. Chem.*, 1974, **52**, 1377.
19. I. J. George, A. Vlasenko, J. G. Slowik, K. Broekhuizen, and J. P. D. Abbatt, *Atmos. Chem. Phys.*, 2007, **7**, 4187–4201.
20. J. D. Hearn, L. H. Renbaum, X. Wang, and G. D. Smith, *Phys. Chem. Chem. Phys.*, 2007, **9**, 4803–13.
21. E. T. Denisov and I. B. Afanas'ev, *Oxidation and Antioxidants in Organic Chemistry and Biology*, Boca Raton, FL, 2005.
22. S. L. Khursan, V. S. Vartem'yanov, and E. T. Denisov, *Kinet. Catal.*, 1989, **31**, 1031–1040.
23. D. Lindsay, J. A. Howard, E. C. Horswill, L. Iton, K. U. Ingold, T. Cobbley, and A. Ll, *Can. J. Chem.*, 1973, **51**, 870.
24. J. D. Smith, J. H. Kroll, C. D. Cappa, D. L. Che, C. L. Liu, M. Ahmed, S. R. Leone, D. R. Worsnop, and K. R. Wilson, *Atmos. Chem. Phys.*, 2009, **9**, 3209–3222.
25. M. Shiraiwa, C. Pfrang, T. Koop, and U. Pöschl, *Atmos. Chem. Phys.*, 2012, **12**, 2777–2794.
26. M. Shiraiwa, M. Ammann, T. Koop, and U. Pöschl, *Proc. Natl. Acad. Sci. U. S. A.*, 2011, **108**, 11003–8.
27. D. Bunker, B. Garrett, T. Kleindienst, and G. L. III, *Combust. Flame*, 1974, **23**, 373–379.
28. D. Gillespie, *J. Phys. Chem.*, 1977, **81**, 2340–2361.
29. G. Wallraff, J. Hutchinson, W. Hinsberg, F. Houle, P. Seidel, R. Johnson, and W. Oldham, *J. Vac. Sci. Technol. B Microelectron. Nanom. Struct.*, 1994, **12**, 3857.
30. F. a. Houle, W. D. Hinsberg, M. Morrison, M. I. Sanchez, G. Wallraff, C. Larson, and J. Hoffnagle, *J. Vac. Sci. Technol. B Microelectron. Nanom. Struct.*, 2000, **18**, 1874.
31. F. A. Houle, W. D. Hinsberg, and M. I. Sanchez, *Macromolecules*, 2002, **35**, 8591–8600.
32. D. T. Gillespie, *J. Chem. Phys.*, 2001, **115**, 1716.
33. W. Hinsberg and F. Houle, *US Pat. 5,625,579*, 1997.
34. F. A. Houle, W. D. Hinsberg, and K. R. Wilson, 2015.
35. S. M. Saunders, M. E. Jenkin, R. G. Derwent, and M. J. Pilling, *Atmos. Chem. Phys.*, 2003, **3**, 161–180.
36. E. Ranzi, M. Dente, A. Goldaniga, G. Bozzano, and T. Faravelli, *Prog. Energy Combust. Sci.*, 2001, **27**, 99–139.
37. E. Ranzi, A. Frassoldati, S. Granata, and T. Faravelli, *Ind. Eng. Chem. Res.*, 2005, **44**, 5170–5183.
38. S. S. Ahmed, F. Mauss, G. Moréac, and T. Zeuch, *Phys. Chem. Chem. Phys.*, 2007, **9**, 1107–26.
39. F. Battin-Leclerc, E. Blurock, R. Bounaceur, R. Fournet, P.-A. Glaude, O. Herbinet, B. Sirjean, and V. Warth, *Chem. Soc. Rev.*, 2011, **40**, 4762–82.
40. E. S. C. Kwok and R. Atkinson, *Atmos. Environ.*, 1995, **29**, 1685–1695.
41. A. Monod and J. F. Doussin, *Atmos. Environ.*, 2008, **42**, 7611–7622.
42. J.-F. Doussin and A. Monod, *Atmos. Chem. Phys.*, 2013, **13**, 11625–11641.
43. L. Vereecken and J. Peeters, *Phys. Chem. Chem. Phys.*, 2009, **11**, 9062–74.
44. S. V Vasenkov, V. A. Bagryansky, W. Korolev, and V. A. Tolkatchev, *Radiat. Phys. Chem.*, 1991, **38**, 191–197.
45. E. Bothe, G. Behrens, and D. Schulte-Frohlinde, *Zeitschrift fur Naturforsch.*, 1977, **32**, 886–889.
46. E. Bothe, M. N. Schuchmann, D. Schulte-Frohlinde, and C. von Sonntag, *Photochem. Photobiol.*, 1978, **28**, 639–643.
47. J. Bennett, *J. Chem. Soc., Faraday Trans.*, 1990, **86**, 3247–3252.
48. E. Villenave, R. Lesclaux, S. Seefeld, and W. R. Stockwell, *J. Geophys. Res.*, 1998, **103**, 25273.
49. J.-P. Le Crâne, E. Villenave, M. D. Hurley, T. J. Wallington, S. Nishida, K. Takahashi, and Y. Matsumi, *J. Phys. Chem. A*, 2004, **108**, 795–805.
50. J.-P. Le Crâne, E. Villenave, M. D. Hurley, T. J. Wallington, and J. C. Ball, *J. Phys. Chem. A*, 2005, **109**, 11837–50.
51. K. U. Ingold, *Acc. Chem. Res.*, 1969, **2**, 1–9.
52. D. Johnson, S. Carr, and R. A. Cox, *Phys. Chem. Chem. Phys.*, 2005, **7**, 2182–90.
53. B. C. Gilbert, P. D. R. Marshall, R. O. C. Norman, N. Pineda, and P. S. Williams, *J. Chem. Soc. Perkin Trans. 2*, 1981, 1392.
54. J. F. Pankow and W. E. Asher, *Atmos. Chem. Phys.*, 2008, **8**, 2773–2796.
55. M. R. Canagaratna, J. L. Jimenez, J. H. Kroll, Q. Chen, S. H. Kessler, P. Massoli, L. Hildebrandt Ruiz, E. Fortner, L. R. Williams, K. R. Wilson, J. D. Surratt, N. M. Donahue, J. T. Jayne, and D. R. Worsnop, *Atmos. Chem. Phys. Discuss.*, 2014, **14**, 19791–19835.
56. S. H. Kessler, J. D. Smith, D. L. Che, D. R. Worsnop, K. R. Wilson, and J. H. Kroll, *Environ. Sci. Technol.*, 2010, **44**, 7005–10.
57. S. H. Kessler, T. Nah, K. E. Daumit, J. D. Smith, S. R. Leone, C. E. Kolb, D. R. Worsnop, K. R. Wilson, and J. H. Kroll, *J. Phys. Chem. A*, 2012, **116**, 6358–65.
58. A. T. Lambe, T. B. Onasch, D. R. Croasdale, J. P. Wright, A. T. Martin, J. P. Franklin, P. Massoli, J. H. Kroll, M. R. Canagaratna, W. H. Brune, D. R. Worsnop, and P. Davidovits, *Environ. Sci. Technol.*, 2012, **46**, 5430–7.
59. A. C. Aiken, P. F. DeCarlo, and J. L. Jimenez, *Anal. Chem.*, 2007, **79**, 8350–8.